Powder Technology 198 (2010) 381–394

Contents lists available at ScienceDirect

Powder Technology

journal homepage: www.elsevier.com/locate/powtec

Empirical description of flow parameters in eccentric flow inside a silo model

Irena Sielamowicz [a,*,1], Michał Czech [b,2], Tomasz A. Kowalewski [c,3]

[a] Białystok Technical University, Civil Engineering Department, 15-351 Bialystok, Wiejska 45 E, Poland
[b] Białystok Technical University, Mechanical Department, 15-351 Bialystok, Wiejska 45 C, Poland
[c] Institute of Fundamental Technological Research, Polish Academy of Sciences, 02-106 Warsaw, Pawinskiego 5B, Poland

ARTICLE INFO

Article history:
Received 12 November 2008
Received in revised form 3 December 2009
Accepted 4 December 2009
Available online 11 December 2009

Keywords:
Methodology
Empirical analysis
DPIV technique
Eccentric granular flow
Discharge on the right
Vertical model
Plexiglas
Velocity
The modified Gauss type function
ch function
Multiple regression

ABSTRACT

The paper presents the methodology of empirical description and statistical analysis of velocity profiles that were depicted by the Digital Particle Image Velocimetry technique (DPIV). Experimental runs were recorded by the high resolution camera in the model with vertical walls. Here we analyze the eccentric discharge with the outlet located in the bottom close to the right vertical wall of the model. On the base of the experimental results we present an empirical analysis of velocities and calculation of the flow rate in two proposed descriptions of the flow. Velocity functions were presented by the exponential function (the modified Gauss type), by the multiple regression and by the ***ch*** function. Also the flow rate was calculated for two presented descriptions. Empirical calculations of the stagnant zone boundary was also presented using the readings from velocity profiles.

1. Introduction

In this paper the methodology of empirical description of velocities, flow rate and stagnant zone boundary on the base of registered velocity fields in eccentric filling and discharge in 2D silo model is presented. In practice even tiny eccentricity of filling or discharge processes may lead to quite an unexpected behaviour of the structure. During asymmetrical processes, flow patterns and wall stresses may be quite different. It is therefore crucial to identify flow patterns developed in the material during eccentric filling or discharge, and to determine both the flow rate and wall stresses occurring under such state of loads. The issues mentioned above are closely related to the flow pattern. Measuring and predicting the pattern of flowing material during discharge were carried out by Cundall and Strack [16], Nedderman and Tüzün [26], Tüzün and Nedderman [44], Haussler and Eibl [19], Runesson and Nilsson [33], Rotter et al. [31]. However, investigation and prediction of the complex flow patterns especially during eccentric discharge still remain a challenge.

2. Literature review

International Standards usually relate to axial symmetric states of stresses and even avoid defining discharge pressures and flow patterns because of continuing uncertainties. In Standard ENV 1991-4 [1], the flow channel geometry and wall pressures under eccentric discharge are defined. The Polish Standard PN-89/B-03262 [4], titled "Silosy żelbetowe na materiały sypkie. Obliczenia statyczne", proposes the values of increased coefficients of horizontal pressure during eccentric discharge. There are codes and guides that include eccentric discharge but they treat it in a different way [2,3,32]. Also a few theoretical solutions have been proposed for the design of silos under eccentric discharge [21,48,29]. The European Standard [1], includes a comment on the eccentricity of the outlet, the definition of the flow channel geometry and the wall pressure under eccentric discharge. Eccentric filling is described as a condition in which the top of the heap at the top of the stored solids at any stage of the filling process is not located on the vertical centreline of the silo. Eccentric discharge is described as a flow pattern in the stored solid arising from moving solid being asymmetrically distributed relative to the vertical centreline of the silo. This normally arises as a result of an eccentrically located outlet

* Corresponding author.
E-mail addresses: sieliren@pb.bialystok.pl (I. Sielamowicz), mceh@pb.bialystok.pl (M.Ł Czech), tkowale@ippt.gov.pl (T.A. Kowalewski).
[1] Tel.: +48 85 7469583; fax: +48 85 7469559.
[2] Tel.: +48 85 7469307; fax: +48 85 7469559.
[3] Tel.: +48 22 826 98 03; fax: +48 22 826 98 03.

0032-5910/$ – see front matter © 2009 Elsevier B.V. All rights reserved.
doi:10.1016/j.powtec.2009.12.003

but can be caused by other asymmetrical phenomena which are not clearly defined. Calculations for flow channel geometry are required for only one size of flow channel contact with the wall, which should be determined for $\Theta_C = 35°$. Other methods of predicting flow channel dimensions may also be used. Wall pressures under eccentric discharge are defined as the pressure on the vertical zone. The pressure depends on the distance "z" below the equivalent solid surface and the frictional traction on the wall at level "z". So far a few approaches have been developed for the design of bins under eccentric discharge [6,29] or by Wood [48]. The issue of eccentricity has also been found to be one of major causes of hopper failures, given by Carson [9]. Eccentricity of the flow to the silo axis causes the pressure patterns to become much more complex than in centric cases. In the field of silo investigations three main issues are analyzed: pressures under eccentric discharge, flow patterns and stagnant zone boundaries. Works on eccentric discharge have been published for many years and a few researchers have dealt with this complicated problem. Anon [5] presented eccentric discharge silo loads and wall loads as a function of discharge rate. Thompson et al. [42] measured wall loads in a corrugated model grain bin when unloaded eccentrically and the effect of eccentric unloading in a model bin for different unloading rates. Pokrant and Britton [28] investigated the effect of eccentricity draw off and flow rate in a model grain bin. Kamiński [22,23] investigated ways of discharge in silo. Hampe and Kamiński [18] analyzed wall pressures under eccentric discharge. Haydl [20] investigated eccentric discharge and the calculation of bending moments in circular silos. They made an experimental study of certain effects of the interaction in the full-scale silo between the reinforced concrete silo walls and a free flowing medium. Safarian and Harris [34] dealt with post-tensioned circular silos for modern industry and presented irregularities of pressure intensity caused by flow problems, eccentric discharge, or multiple discharge openings. Rotter et al. [30] discussed experiments with buckling failure problems in which the wall stresses were directly induced by stored solids. De Clercq [15] studied flow patterns in a silo with concentric and eccentric outlet, and also a steel silo with two types of outlets and its susceptibility to buckling. He found that a thin-walled silo with concentric outlet tends to be well behaved, and whereas the other one with eccentric outlet was susceptible to buckling and collapse. It was also stated that none of the existing theories adequately addressed the issue of buckling of eccentrically-emptied silos. Blight [7] investigated the behaviour of two steel silos under eccentric discharge. Borcz et al. [8] presented experimental results of pressure measurements in the wall in a full-scale silo under eccentric discharge. Shalouf and Kobielak [35] analyzed eccentric discharge in silos and reduction of the dynamic flow pressures in grain silo by using discharge tubes. Ayuga et al. [6] investigated discharge and the eccentricity of the hopper influence on silo wall pressures. Molenda et al. [25] presented investigations on bin loads by both central and eccentric filling and discharge of grains in a model of silo. In the analysis, Chou et al. [13] using the kinematic model, proposed by Nedderman and Tüzün [26], constructed a boundary-value problem. The results consist of measurements of circumferential shell wall deformation for various load histories as a function given service cycles: filling and discharge — centrally and eccentrically. Chou et al. [13] investigated granular flow in a two-dimensional flat-bottomed hopper with eccentric discharge. Wójcik et al. [47] presented numerical analysis of wall pressures in silos with concentric and eccentric hoppers. Chou et al. [12] made some experiments in a two-dimensional flat-bottomed model and identified flow patterns and stresses on the wall during centric and eccentric discharge. The flowing material was recorded using a digital camcorder and the normal and shear stresses were measured using pressure gauges. Chou and Hsu [14] measured experimentally the heights of the stagnant zones for two kinds of granular materials after hopper eccentric and centric discharge. Guaita et al. [17] applied FEM modelling in the analysis of influence of hopper eccentricity on wall pressures. In the proposed model the distribution of plastic areas according to eccentricity was analyzed. Song and Teng [39] analyzed the results in FEM of a buckling strength of steel silo subject to code-specified pressures for eccentric discharge with the wall loads predicted by four codes where the pressure asymmetry was determined by local pressure increases or reductions and described by the authors as patch loads. Nübel and Huang [27] presented a study of localized deformation pattern in granular materials, investigating shear localizations in granular materials numerically, with the use of a Cosserat continuum approach, and compared the obtained results to experimental data. Tejchman [40,41] also presented a numerical Cosserat approach to the behaviour of granular medium in a silo.

The latest paper on the flow pattern measurement however, in a full-scale silo not in a model, was presented by Chen et al. [10]. One can find a long list of references concerning investigation of eccentric discharge there.

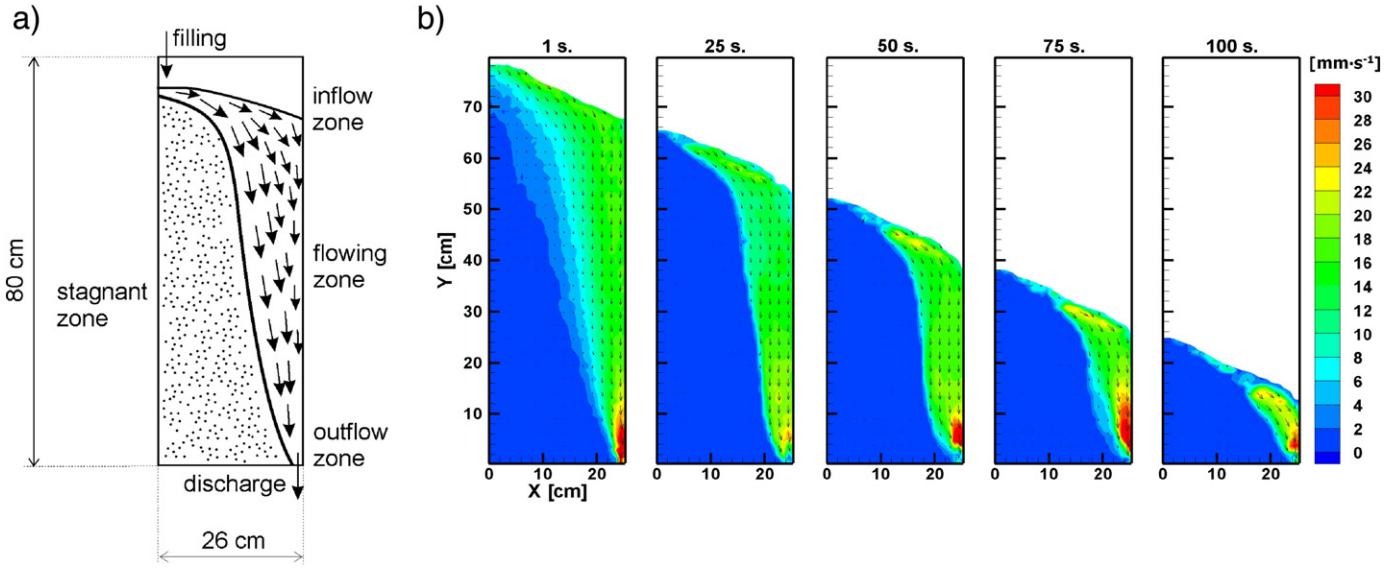

Fig. 1. Eccentric flow of flax seed: filling from the left and discharge from the right, a) flow mode formed in the model, b) velocity contours.

3. Results of experimental investigations used to empirical analysis

The experimental setup used in the experiments was presented in Sielamowicz et al. [36,37]. Recording the flow in the model of depth 10 cm the high-speed CCD camera (PCO1200HS) with the objective 50 mm lens was used. Sequences of 12-bit images with the resolution of 1280×1024 pixels were acquired by Pentium 4 based personal

Table 1
Values of the symbols given in formula (2).

Parameters	$i=0$	$i=1$	$i=2$
A_i	3.679	−0.062143	0.000803132
B_i	0.065893	0.0081573	−0.000165805
C_i	−0.10255	0.0035087	−0.000031846

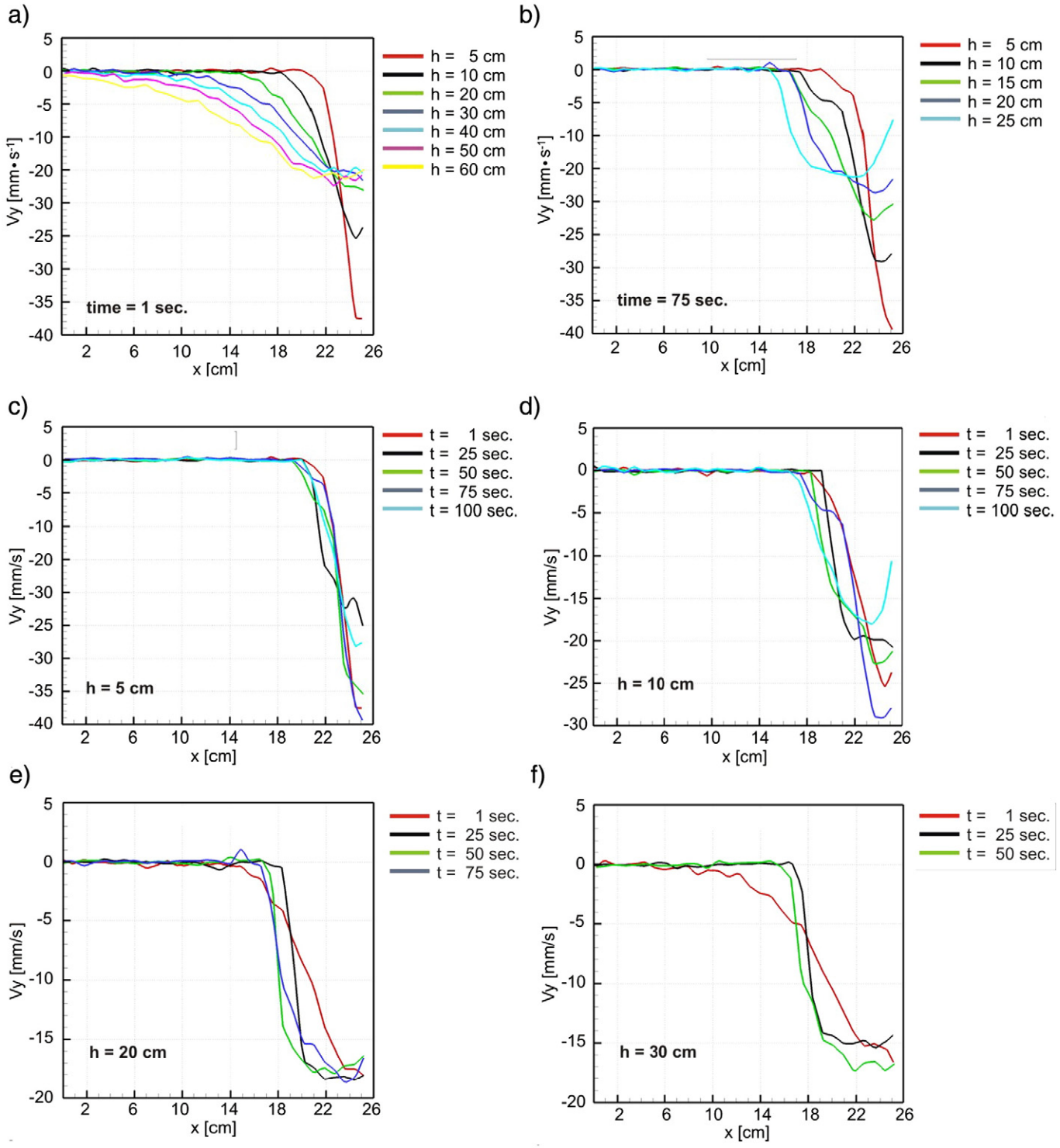

Fig. 2. Velocity profiles of flax seed flow at: various time instants (a–b) and levels (c–f).

Table 2
Values of coefficients a_i in formula (3).

a_0	a_1	a_2	a_3	a_4	a_5	a_6	a_7	a_8	R coefficient of correlation
3.663	$-49.92\ 10^{-3}$	$0.577\ 10^{-3}$	$-143.42\ 10^{-3}$	$3.159\ 10^{-3}$	$-0.184\ 10^{-3}$	$-45.704\ 10^{-3}$	$0.886\ 10^{-3}$	$-0.003\ 10^{-3}$	0.9714

computer using IEEE1394 interface. The system allowed to acquire up to 1000 images at time interval of 1.5 ms (667 fps). The velocity field was evaluated for triplets of images using the DPIV based on the Optical Flow technique, Quenot et al. [50]. Dense velocity fields with vectors for each pixel of the image were obtained and used for further evaluation of the velocity profiles, velocity contours and streamlines. The term "streamline" is defined as a direction of the flow of different particles at the same time. Intrinsic resolution of the PIV technique is limited by the size of the area of interest that is used in the application of the cross correlation algorithm between subsequent images and this is generally one order of magnitude larger than a single pixel. An Optical Flow technique based on the use of Dynamic Programming [Quenot et al. [50]] has been applied to Particle Image Velocimetry thus yielding a significant increase in the accuracy and spatial resolution of the velocity field. A velocity vector is obtained for every pixel of the image and typical for classical PIV constrains are removed. Calibration carried out for synthetic sequences of images shows that the accuracy of measured displacement is about 0.5 pixel/frame for tested two-image sequences and 0.2 pixel/frame for four-image sequences.

Table 3
Parameters A, B and C in formula (4), the 1st regression.

Level H [cm]	A	B	C
5	4.1800	0.10689	−0.10904
10	3.7170	0.11379	−0.048339
20	3.2350	0.38199	−0.066509
30	3.3078	0.15780	−0.028827
40	3.0010	0.20549	−0.024767
50	3.2337	0.040317	−0.0088796
60	3.4154	0.031379	−0.0070211

Table 4
Values of the parameters in formula (2).

Parameters	$i=0$	$i=1$	$i=2$
A_i	4.396	−0.068208	0.00087487
B_i	0.06613	0.012485	−0.00023117
C_i	−0.10702	0.0032341	$-2.62531\ 10^{-5}$

Slominski et al. [38] presented a detailed description of PIV technique with its advantages and disadvantages. The aim of the present investigation is to explore the possibility of using the Optical Flow technique based on PIV in measuring granular material flow velocity. In this paper we apply the Optical Flow technique DPIV to investigate dynamic behaviour of granular material during discharge and measure flow profiles, velocity distributions, vector fields in plane flow hoppers with eccentric filling and discharge. In order to evaluate velocity long sequences of 100–400 images were taken at variable time intervals covering the whole discharge time. In granular material flow one usually visualizes a track of individual particles, not necessarily coinciding with the streamline. Such tracks were obtained by Choi et al. [11], who used a high-speed imaging technique to trace the position of single particles in granular materials. Velocity profiles obtained that way for the flow of granular material inside a quasi-two-bottomed silo were smooth and free of shock-like discontinuities. In contrast, the DPIV technique used here produces velocity field for the full interrogation area, and this can be used to predict the natural track of individual particles.

4. Theoretical description of velocities

We present here the methodology of theoretical analysis of velocities in asymmetric flow of flax seed in the model with vertical and smooth walls with outlet located close to the right wall. We consider the case discussed in Fig. 1 where the flow mode is also presented. The model has the depth of 5 cm. Properties of the granular material used in the experiment: angle of wall friction against Plexiglas $\varphi_w = 26^o$, angle of internal friction $\varphi_e = 25^o$, Young modulus $E = 6.11$ MPa, granular material density deposited through a pipe with zero free-fall $\rho_b = 746$ kg/m^3 at 1 kPa and 747 kg/m^3 at 8 kPa.

Fig. 2 presents selected velocity profiles obtained for the case of filling made from the left and with discharge outlet located near the right wall. The readings taken from the velocity profiles are presented in Tables 1–7 published in Appendix.

Statistical analysis of the experimental results with application of the values given in Tables 1–7 (published in Appendix) was done. The confidence intervals for the averages were determined for the analyzed levels and are listed in Tables 8–13 published in Appendix

Table 5
Values of coefficients a_i in formula (5).

a_0	a_1	a_2	a_3	a_4	a_5	a_6	a_7	a_8	R coefficient of correlation
4.2904	−0.04908	0.000552	−0.052342	0.01143	−0.00017	−0.062328	0.001345	−0.000007	0.9695

Table 6
Sums of the squares of the differences of velocities.

Regression	Sums of the squares of the differences of velocities measured at the analyzed levels $\sum(V_{emp}-\overline{V}_{y\,\mathrm{exp}})^2$							
	5 cm	10 cm	20 cm	30 cm	40 cm	50 cm	60 cm	$\sum\sum(V_{emp}-\overline{V}_{y\,\mathrm{exp}})^2$
Generalized Gauss description								
1st	10.208	3.490	40.234	10.959	6.118	39.354	11.496	121.85
2nd	35.304	62.223	136.29	17.591	170.465	198.620	169.803	790.30
Multiple	101.645	63.307	70.573	14.221	18.828	30.752	38.005	337.33
$\sum\sum$	147.157	129.020	247.097	42.771	195.411	268.726	219.294	1249.48
Generalized the ***ch*** *function description*								
1st	6.299	3.153	76.849	13.041	9.213	22.865	4.992	136.41
2nd	31.151	50.542	63.660	32.277	136.013	147.475	150.124	611.24
Multiple	95.186	38.688	64.369	18.055	12.628	24.568	29.405	282.90
$\sum\sum$	132.636	92.383	204.878	63.373	157.854	194.908	184.521	1030.55

[46]. The averages were calculated using the sums of the columns in Tables 1–6. In the calculations the flow time was not taken into account. In this analysis there are no readings that were removed from the data set.

4.1. Description of velocities by the exponential function (generalized, the Gauss type)

At the beginning of the analysis the vertical velocity component V_y was depended on two factors: the distance x — the location of the measurement points and also on the various heights z. The type of the function applied in the empirical description of vertical velocity V_y calculated in millimetres per second was proposed as the following:

$$V_y = e^{A + Bx + Cx^2} \tag{1}$$

where parameters A, B and C were determined by the least squares method (*the first regression*), presented in the form of points in Fig. 3. The solid lines show the empirical description of these parameters at various analyzed levels.

Parameters A, B and C were depended on the height z in the model according to formula (2). Analyzing the distribution of parameters A, B and C we can expect the second regression results to be less agreed with the experimental results (cf. Fig. 4). Thus, calculating the second regression, the shape of the function to describe velocity V_y by the multiple regression was determined:

$$\begin{aligned} \hat{A} &= A_0 + A_1 z + A_2 z^2 \\ \hat{B} &= B_0 + B_1 z + B_2 z^2 \\ \hat{C} &= C_0 + C_1 z + C_2 z^2. \end{aligned} \tag{2}$$

Parameters A_i, B_i, and C_i for $i = 0, 1, 2$ were obtained by the least squares method using formula (2) and are listed in Table 1.

On the basis of formulas (1) and (2) and the values listed in Table 1, velocity distributions were drawn. Fig. 4 presents the comparison of the average experimental results $\overline{V_y}$ exp with empirical values $\hat{V}_y empir$ after the 1st regression (depending the velocity on the distance from the symmetry axis x), after the 2nd regression $\hat{\hat{V}}_y empir$, depending the velocity both on the distance x and on the height z and after the multiple regression $\hat{\hat{\hat{V}}}_y$ that is discussed in the next section.

4.2. Description of velocities by the multiple regression

Applying the 1st and the 2nd regression, the description of vertical velocity was assumed in the form of the following function:

$$V_y = \exp(a_0 + a_1 x_1 + a_2 x_2 + a_3 x_3 + a_4 x_4 + a_5 x_5 + a_6 x_6 + a_7 x_7 + a_8 x_8) \tag{3}$$

where

$$x_1 = z,\ x_2 = z^2,\ x_3 = x,\ x_4 = xz,\ x_5 = xz^2,\ x_6 = x^2,\ x_7 = xz^2,\ x_8 = z^2 x^2$$

and x denotes the distance from the left wall, z — is the height of the analyzed level in the model, measured in centimetres. The coefficients a_1 where $i = 0, 1 \ldots 8$ were calculated by the least squares method, and are listed in Table 2. We define the calculations accurately using the multiple regression. There is a possibility to determine the parameters by the nonlinear regression, that would define the description a little more accurately.

On the basis of formula (3) and data listed in Table 2, the values of vertical velocity $\hat{\hat{\hat{V}}}_y$ were calculated. Three approaches of describing the velocity in the model presented above are shown in Fig. 4. The points relate to the average values of experimental measurements and the solid lines represent the functional descriptions of velocity after the 1st ($\hat{V}_y$), the 2nd ($\hat{\hat{V}}_y$) and the multiple regression ($\hat{\hat{\hat{V}}}_y$).

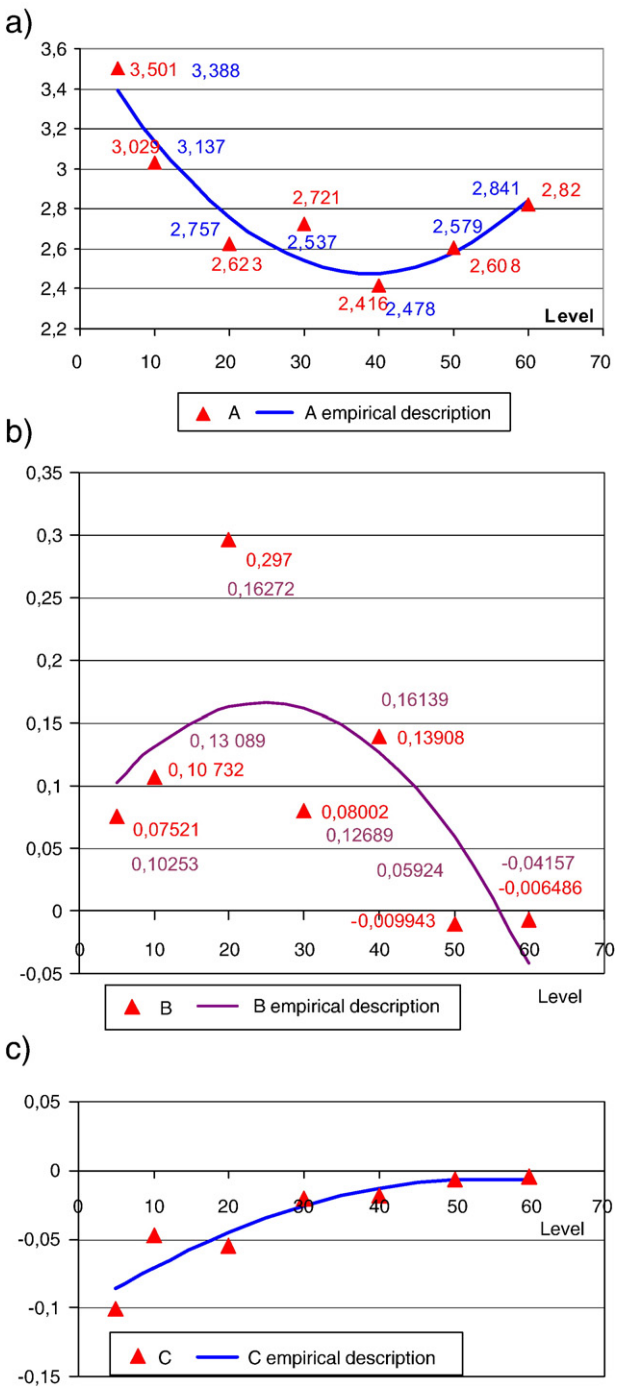

Fig. 3. Distributions of parameters A, B and C (points) and their empirical descriptions (solid lines).

It should be stated that there is a problem to find a proper form of the function that would describe velocity in the model but the type of the function given in formulas (1) and (2) describes the distribution of velocity quite well, especially in determining the parameters by the multiple regression. We have also found the best description of velocities for the lowest levels at $H = 5$ cm and $H = 10$ cm. The higher the level is located the higher regression should be applied to describe the velocities. But it is not a rule. This is changing at the middle levels.

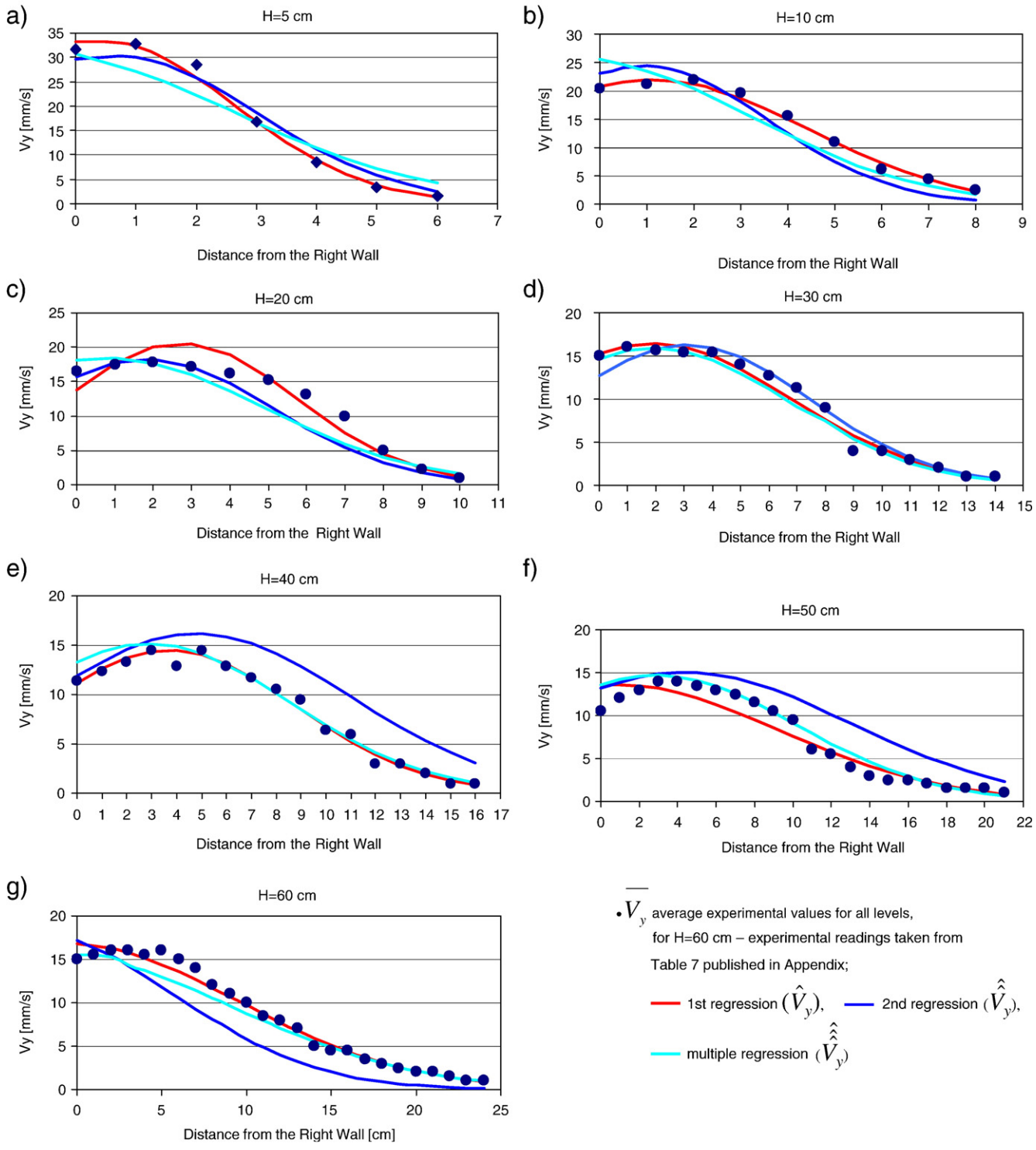

Fig. 4. Velocity distributions: average experimental results compared with the 1st, the 2nd and the multiple regression.

Velocity distributions (cf. Fig. 4) confirm the aptness of the applied function for the multiple regression.

4.3. Description of velocities by the generalized ***ch*** function

In this section we propose another empirical description of velocity by the ***ch*** function in the following form:

$$V_y = ch(A + Bx + Cx^2). \quad (4)$$

In this analysis the velocity was depended on the distance x using the 1st regression. Parameters A, B and C in the empirical description were calculated by the least squares method and are listed in Table 3.

Parameters A, B and C in formula (4) are depended on the height z as was presented in formula (2). Coefficients A_i, B_i and C_i calculated by the least squares method are listed in Table 4. Their parabolic descriptions are presented in Fig. 5. Using formulas (2) and (4) and values listed in Table 4 we obtain the description of velocity dependent on the distance x and the height z after the second regression.

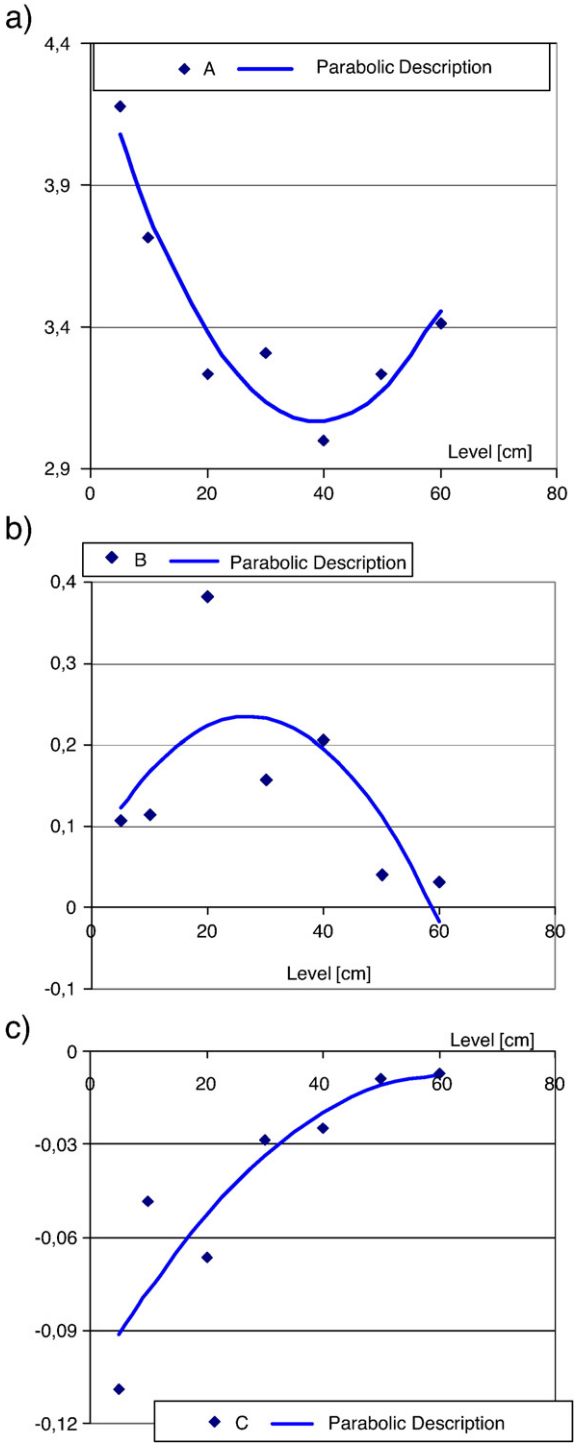

Fig. 5. Distribution of parameters *A*, *B* and *C*.

On the basis of the 1st and 2nd regressions we assumed the vertical velocity in the form:

$$V_y = ch(a_0 + a_1x_1 + a_2x_2 + a_3x_3 + a_4x_4 + a_5x_5 + a_6x_6 + a_7x_7 + a_8x_8). \quad (5)$$

Parameters a_1 where $i=0,1,2\ldots8$ were calculated by the least squares method, and listed in Table 5. Variables x_1, x_2, x_3, x_4, x_5, x_6, x_7, and x_8 were applied like in formula (3).

Applying the approaches presented above we show the vertical velocity distributions in Fig. 6. Description of velocities by the ***ch*** function also proved that at the higher levels the best agreement of the experimental and empirical results was obtained by the first and the multiple regression. The second regression was only needed to predict the type of the function to describe velocity.

4.4. Verification of the accuracy of the applied descriptions

We also verified the accuracy of the applied descriptions. In Table 6 the sums of the squares of the differences of velocities in three applied regressions by the Gauss description and by the ***ch*** function are presented.

As it is seen the best description of velocities was found using the ***ch*** function because the sum of the sums of the squares is lower, both in the used regressions and at the analyzed levels.

4.5. Flow rate

The flow rate Q was calculated for two presented descriptions of velocities. In the solution given by the Gauss exponential function the flow rate was calculated according to the following formula:

$$Q = \int_0^{x_n} e^{A + Bx + Cx^2} dx \quad (6)$$

and the values of Q are listed in Table 7. In formulas (6) and (8) the limit of integration x_n denotes the distance of the last measurement point from the right wall taken from the experimental readings for various analyzed levels (cf. Tables 1–7 published in Appendix). The flow rate was described by the following parabolic function:

$$\tilde{Q} = \tilde{A}_1 + \tilde{B}_1 z + \tilde{C}_1 z^2 \quad (7)$$

where parameters $\tilde{A}_1 = 110.54$, $\tilde{B}_1 = -0.20605$, and $\tilde{C}_1 = 0.26017$ were calculated by the least squares method using the values listed in Table 7. On the basis of parameters $\tilde{A}_1$, $\tilde{B}_1$, and $\tilde{C}_1$, the values of the flow rate $\tilde{Q}$ were determined and these values were used in calculations of the sums of the squares of the differences that are also listed in Table 7.

In the description of velocities by the ***ch*** function, the flow rate was calculated according to the formula:

$$Q = \int_0^{x_n} ch(A + Bx + Cx^2) dx \quad (8)$$

and the values are listed in Table 7. The limit of integration x_n was taken like in formula (6). The flow rate $\tilde{Q}$ was also described by the parabolic function given in formula (7) and parameters $\tilde{A}_2 = 110.18$, $\tilde{B}_2 = -0.076199$, and $\tilde{C}_2 = 0.024345$ were determined by the least squares method using the values listed in Table 7. On the basis of the values of parameters $\tilde{A}_2$, $\tilde{B}_2$, and $\tilde{C}_2$, the values of the flow rate $\tilde{Q}$ were calculated and used to determine the sums of the squares of the differences of velocities that are also listed in Table 7.

In both solutions the parameters $\tilde{A}_i$, $\tilde{B}_i$, and $\tilde{C}_i$ for $i=1,2$, were introduced into the analysis after the 1st regression, from Fig. 3 and Table 3, respectively. The best description of the flow rate was obtained by the Gauss function, because the sum of the sums of the differences of velocities given in Table 7 is lower than in the case of the description made by the ***ch*** function (Fig. 7).

In the two presented cases the calculated values of the flow rate $Q\cdot[\mathrm{cm}^2/\mathrm{s}]$ are almost similar, both in the empiric description (by the parabolic function) and by the integrated values using formulas (6) and (8), respectively. In the region between the level $H=5$ cm and the level $H=10$ cm where the flow channel is the narrowest (cf. Fig. 1), the increase of the flow rate reaches approximately the similar values. From this level the increase of the flow rate is rapid. From level $H=20$ cm up and higher the increase of the flow rate is not constant. As a result of differentiating formula (7) we obtain the linear increment of the velocity of the flow rate at different levels. The difference of the flow rate reaches 0.352 [cm^2/s] between levels $H=20$ cm and $H=30$ cm and 1.053 [cm^2/s]

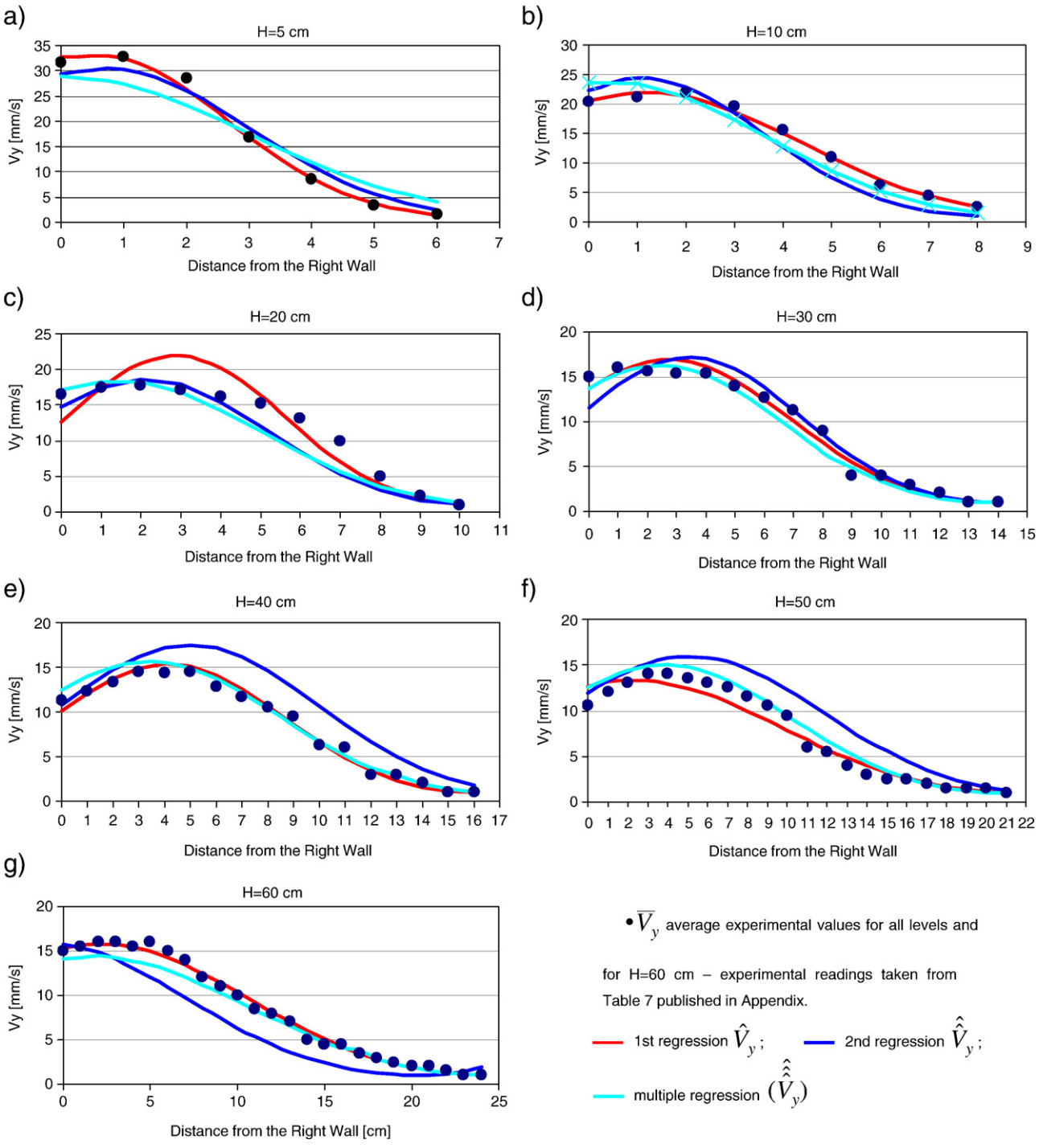

Fig. 6. Vertical velocity descriptions by the three applied methods.

Table 7
Values of the flow rate (integrated).

Level H [cm]	x_n [cm]	Q [cm^2/s]		Sums of the squares of differences $\sum(Q_{empir}-\tilde{Q})^2$	
		Generalized Gauss description	Description by the generalized ***ch*** function	Generalized Gauss description ($\times 10^{-2}$)	Description by the generalized ***ch*** function ($\times 10^{-2}$)
5	6	10.51	10.565	25.6036	22.6576
10	8	11.116	11.120	0.0064	0.4356
20	10	12.655	12.859	94.4784	103.8361
30	14	13.007	13.229	5.2441	6.1504
40	16	14.06	14.301	11.0889	9.4864
50	21	15.363	15.467	135.7225	158.0049
60	24	19.979	20.165	63.2025	302.4121
$\sum\sum$				335.3464	602.9831

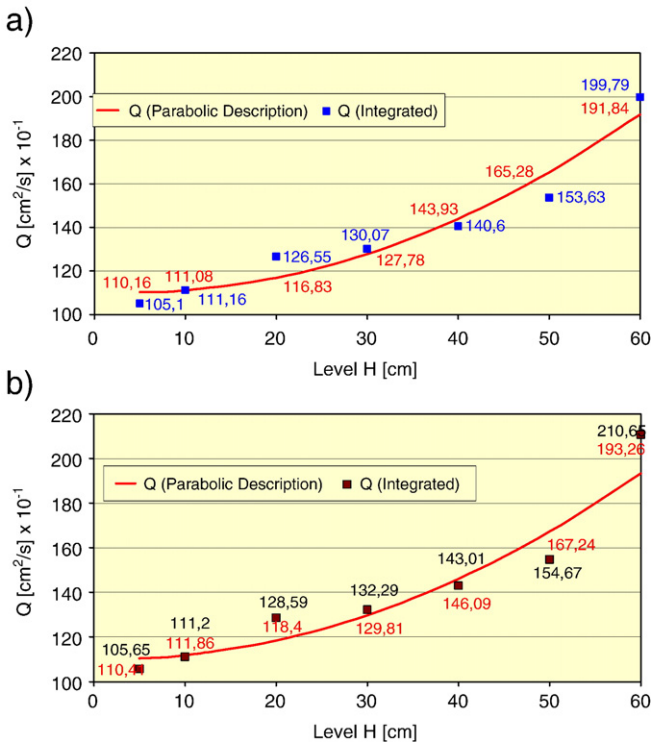

Fig. 7. Comparison of the flow rate calculated by: a) the function of the Gauss type, b) the ***ch*** function.

between levels $H=30$ cm and $H=40$ cm, respectively. But higher than $H=40$ cm the flow rate increases more rapidly because the flow channel widens, thus more material flows into it with higher velocity. The increase of the flow rate between level $H=40$ cm and $H=50$ cm is again lower and reaches 1.303 [cm^2/s] and between level $H=50$ cm and $H=60$ cm is already 4.616 [cm^2/s]. The flow channel at level $H=50$ cm is so wide that the flow rate reached more than 15.0 [cm^2/s].

5. Empirical determination of stagnant zone boundary

Basing on the readings listed in Tables 1–7 given in Appendix, the distances x_i (for instance $x=2$, 3, 4, and 5 cm) were determined from the right wall of the model. And the last four readings of velocities V_y of nonzero values were taken for the analysis. Velocities V_y were depended on x by the functions of: the parabolic type $\hat{V}_y=A_1+B_1x+C_1x^2$, hyperbolic type $\hat{V}_y = A + \frac{B}{x}$, or linear type $\hat{V}_y=a+bx$. We searched the values x at which $V_y=0$ (stagnant zone boundary). At first we applied the parabola of the second order to approximate the four chosen experimental readings of vertical velocity V_y. If we do not obtain the zero values of velocities in the assumed approximation then we should apply another function to approximate the experimental values of velocities V_y. From these two functions only one can be chosen for which the coefficient of correlation has the highest value. The choice of the parabolic function for the first approximation came out from the fact that the more there are constant coefficients in the description of the function, the more accurate description should be expected. Here we approximated values of velocities by the three proposed types of the functions and we obtained values x for which $V_y=0$ (stagnant zone boundary). Several authors defined the stagnant zone boundary in a various way: Zhang and Ooi [49] called it as the flow channel boundary (FCB), as the zone in which the particles do not slough off the solids surface but follow the paths predicted by the kinematic theory all the way to the outlet. The particles located in the surrounding feeding zone

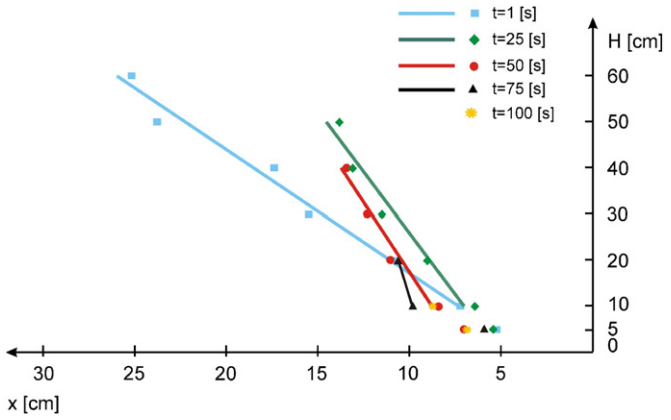

Fig. 8. Range of the stagnant zone boundary at the analyzed instants of the flow.

enter the top flow layer and roll down to the central axis and then finally move towards the outlet. Many numerous investigations at measuring and predicting the pattern of material flow during silo discharging have been carried out (e.g. [16,26]). Tüzün and Nedderman [43] defined the flow channel boundary as the streamline within which 99% of the total flow takes place while Watson and Rotter [45] proposed to define the boundary where the velocity at each level is 1% of the centre line velocity at that level. In the case of asymmetric flows the maximal velocities occur in various distances from the right wall of the model. Hence $V_y=0$ was assumed at the stagnant zone boundary. The values of x and the parameters of the proposed functions are given in Table 14 in Appendix. On the basis of these data, the points of the calculated values of x at which vertical velocity $V_y=0$ are shown in Fig. 8.

The regression lines determined on the basis of the data given in Table 14 (Appendix) are also shown in Fig. 8. The equations of these lines were calculated for the height $H\geq 10$ cm and they are the following:

$$\begin{aligned}
&- \text{ for 1 } s \text{ of the flow } \hat{x} = 3.58 + 0.3733H;\ r = 0.990\\
&- \text{ for 25th } s \text{ of the flow } \hat{x} = 5.12 + 0.1884H;\ r = 0.979\\
&- \text{ for 50th } s \text{ of the flow } \hat{x} = 7.21 + 0.163H;\ r = 0.974\\
&- \text{ for 75th } s \text{ of the flow } \hat{x} = 9.08 + 0.076H;\ r = 1.
\end{aligned} \tag{9}$$

In the presented analysis we described the distribution of the range of the stagnant zone boundary forming in the flowing material from the level $H=10$ cm up. For heights $H\geq 10$ cm it is possible to approximate the stagnant zone boundary by the line. This fact is confirmed by the coefficients of correlation given in formula (9).

6. Conclusions

In the presented empirical analysis of velocities in the flowing material in the model with eccentric filling and discharge we applied two types of functions to describe velocities. We have found that both the function of the generalized Gauss type and the ***ch*** function decrypt velocities in dependence on variables x and z, especially calculating the parameters of the empirical functions using the multiple regression. However to find such type of the function (i.e. to depend velocity both on x and z) first we had to apply two single regressions. Having the values of the flow rate shown in Fig. 7a and b, described by 2° parabola we can investigate the flow rate at lower levels and by extrapolating the function we can predict the values of the flow rate at higher levels. In the paper we presented the way on how to predict the stagnant zone boundary. It was assumed at the boundary velocity $V_y=0$. We did not apply the value of vertical velocity V_y at the boundary equal to 1% of the maximal velocity because the maximal values of velocity appear in different distances from the lateral wall of the model. Further work is required to investigate the stagnant zone boundary location in asymmetrical flows.

Acknowledgements

The authors express their deep gratitude to Prof. Zenon Mróz of the Fundamental Technological Research of Polish Academy of Sciences in Warsaw for all suggestions concerning the analysis of the problem presented in this paper. All experiments in DPIV technique were performed at the Department of Mechanics and Physics of Fluids at the Institute of Fundamental Technological Research of Polish Academy of Sciences in Warsaw. Special thanks direct to Mr Sławomir Błoński for providing numerical results in DPIV technique. The paper was partly prepared under the Rector's Project W/IIB/11/06 and S/WM/2/08.

Appendix A. Empirical analysis of the flow of the flax seed in the model with smooth walls. Discharge from the right

Table 1
Readings at level $H=5$ cm.

Time [s]	Velocities V_y [mm/s] at the distance from the symmetry axis x [cm]						
	0	1	2	3	4	5	6
1 s	36.0	37.0	30.0	15.0	5.0	1.0	0
25 s	23.0	25.0	22.0	20.0	16.0	5.0	0
50 s	34.0	35.0	33.0	17.0	8.0	6.0	2.0
75 s	38.0	39.0	32.0	17.0	5.0	3.0	1.0
100 s	27.0	28.0	25.0	15.0	9.0	2.0	0

Table 2
Readings at level $H=10$ cm.

Time [s]	Velocities V_y [mm/s] at the distance from the symmetry axis x [cm]								
	0	1	2	3	4	5	6	7	8
1 s	24.0	25.0	22.0	17.0	11.5	4.0	3.0	1.0	0
25 s	21.0	20.0	19.0	20.0	20.0	17.0	6.0	0	0
50 s	20.0	21.0	23.0	19.0	17.0	15.0	8.0	6.0	0
75 s	28.0	29.0	29.0	25.0	13.0	6.0	4.0	4.0	2.0
100 s	9.0	11.0	17.0	17.0	16.0	13.0	10.0	7.0	3.0

Table 3
Readings at level $H=20$ cm.

Time [s]	Velocities V_y [mm/s] at the distance from the symmetry axis x [cm]										
	0	1	2	3	4	5	6	7	8	9	10
1	17.0	18.0	17.0	15.0	13.0	11.0	9.0	6.0	4.0	2.0	1.0
25	17.0	18.0	18.0	18.0	18.0	17.0	13.0	8.0	1.0	0	0
50	16.0	17.0	17.0	17.5	17.0	18.0	16.5	15.0	8.0	0	0
75	16.0	17.0	19.0	18.0	17.0	15.0	14.0	11.0	7.0	2.5	0

Table 4
Readings at level $H=30$ cm.

Time [s]	Velocities V_y [mm/s] at the distance from the symmetry axis x [cm]															
	0	1	2	3	4	5	6	7	8	9	10	11	12	13	14	15
1	15.0	16.0	15.0	14.0	14.0	11.0	9.0	7.0	6.0	5.0	4.0	3.0	2.0	1.0	1.0	0
25	14.0	15.0	15.0	15.0	15.0	15.0	14.0	13.0	10.0	2.0	0	0	0	0	0	0
50	16.0	17.0	17.0	17.0	17.0	16.0	15.0	14.0	11.0	5.0	0	3.0	0	0	0	0

Table 5
Readings at level $H=40$ cm.

Time [s]	Velocities V_y [mm/s] at the distance from the symmetry axis x [cm]																
	0	1	2	3	4	5	6	7	8	9	10	11	12	13	14	15	16
1	14.0	15.0	15.0	15.0	15.0	14.0	12.5	11.0	9.0	7.0	6.0	5.0	4.0	3.0	2.0	1.0	1.0
25	13.0	14.0	15.0	14.0	14.0	13.5	12.0	11.0	10.0	9.0	2.0	0	0	0	0	0	0
50	7.0	8.0	10.0	14.5	14.0	16.0	14.0	13.0	12.5	12.5	11.0	7.0	2.0	0	0	0	0

Table 6
Readings at level $H = 50$ cm.

Time [s]	Velocities V_y [mm/s] at the distance from the symmetry axis x [cm]																					
	0	1	2	3	4	5	6	7	8	9	10	11	12	13	14	15	16	17	18	19	20	21
1	15.0	16.0	16.0	17.0	16.0	15.0	14.0	13.0	11.0	10.0	9.0	7.0	5.0	4.0	3.0	2.5	2.5	2.0	1.5	1.5	1.5	1
25	6.0	8.0	10.0	11.0	12.0	12.0	12.0	12.0	12.0	11.0	10.0	5.0	0	0	0	0	0	0	0	0	0	0

Table 7
Readings at level $H = 60$ cm.

Time [s]	Velocities V_y [mm/s] at the distance from the symmetry axis x [cm]																							
	0	1	2	3	4	5	6	7	8	9	10	11	12	13	14	15	16	17	18	19	20	21	22	23	24
1	15.0	15.5	16.0	16.0	15.5	16.0	14.0	14.0	12.0	11.0	10.0	8.0	8.5	7.0	5.0	4.5	4.5	3.5	3.0	2.5	2.0	2.0	1.5	1	1

Statistical analysis of the experimental results

Table 8
Statistical values for calculation of the confidence interval for level $H = 5$ cm.

Distance from the symmetry axis [cm]	$x=0$	$x=1$	$x=2$	$x=3$	$x=4$	$x=5$	$x=6$
Statistical values							
$\overline{V_y}$	31.6	32.8	28.4	16.8	8.6	3.4	1.5
S	5.678	5.381	4.224	1.833	4.030	1.855	0.5
n	5	5	5	5	5	5	2
$t_{n-1,1-\frac{\alpha}{2}}$	2.7764	2.7764	2.7764	2.7764	2.7764	2.7764	12.706
$t_{n-1,1-\frac{\alpha}{2}}\frac{S}{\sqrt{n-1}}$	7.88	7.47	5.86	2.54	5.59	2.58	6.35
$\overline{V_y}-t_{n-1,1-\frac{\alpha}{2}}\frac{S}{\sqrt{n-1}}$	23.72	25.33	22.54	14.26	3.01	0.82	0
$\overline{V_y}+t_{n-1,1-\frac{\alpha}{2}}\frac{S}{\sqrt{n-1}}$	39.48	40.27	34.26	19.34	14.19	5.98	7.85

Table 9
Statistical values for calculation of the confidence interval for level $H = 10$ cm.

Distance from the symmetry axis [cm]	$x=0$	$x=1$	$x=2$	$x=3$	$x=4$	$x=5$	$x=6$	$x=7$	$x=8$
Statistical values									
$\overline{V_y}$	20.4	21.2	22.0	19.6	15.5	11.0	6.2	4.5	2.5
S	6.344	6.013	4.099	2.939	3.0	5.099	2.561	2.291	0.5
n	5	5	5	5	5	5	5	4	2
$t_{n-1,1-\frac{\alpha}{2}}$	2.7764	2.7764	2.7764	2.7764	2.7764	2.7764	2.7764	3.1824	12.706
$t_{n-1,1-\frac{\alpha}{2}}\frac{S}{\sqrt{n-1}}$	8.81	8.35	5.69	4.08	4.16	7.08	3.56	4.21	6.35
$\overline{V_y}-t_{n-1,1-\frac{\alpha}{2}}\frac{S}{\sqrt{n-1}}$	11.59	12.85	16.31	15.52	11.34	3.92	2.64	0.29	0
$\overline{V_y}+t_{n-1,1-\frac{\alpha}{2}}\frac{S}{\sqrt{n-1}}$	29.21	29.55	27.69	23.68	19.66	18.08	9.76	8.71	8.85

Table 10
Statistical values for calculation of the confidence interval for level $H = 20$ cm.

Distance from the symmetry axis [cm]	$x=0$	$x=1$	$x=2$	$x=3$	$x=4$	$x=5$	$x=6$	$x=7$	$x=8$	$x=9$	$x=10$	$x=11$
Statistical values												
$\overline{V_y}$	16.5	17.5	17.75	17.125	16.25	15.25	13.125	10.0	5.0	2.25	1	1
S	0.5	0.5	0.829	1.244	1.920	2.681	2.701	3.391	2.739	0.25	1	–
n	4	4	4	4	4	4	4	4	4	2	1	–
$t_{n-1,1-\frac{\alpha}{2}}$	3.1824	3.1824	3.1824	3.1824	3.1824	3.1824	3.1824	3.1824	3.1824	12.706		
$t_{n-1,1-\frac{\alpha}{2}}\frac{S}{\sqrt{n-1}}$	0.92	0.92	1.52	2.29	3.53	4.93	4.96	6.23	5.03	3.18		
$\overline{V_y}-t_{n-1,1-\frac{\alpha}{2}}\frac{S}{\sqrt{n-1}}$	15.58	16.58	16.23	14.84	12.72	10.32	8.17	3.77	0	0		
$\overline{V_y}+t_{n-1,1-\frac{\alpha}{2}}\frac{S}{\sqrt{n-1}}$	17.42	18.42	19.27	19.42	19.78	20.18	18.09	16.23	10.03	5.43		

Table 11
Statistical values for calculation of the confidence interval for level $H = 30$ cm.

Distance from the symmetry axis [cm]	$x=0$	$x=1$	$x=2$	$x=3$	$x=4$	$x=5$	$x=6$	$x=7$	$x=8$	$x=9$	$x=10$	$x=11$	$x=12$	$x=13$	$x=14$
Statistical values															
$\overline{V_y}$	15.0	16.0	15.67	15.33	15.33	14.0	12.67	11.33	9.0	4.0	4.0	3.0	2.0	1.0	1.0
S	0.816	0.816	0.943	1.247	1.247	2.16	2.625	3.091	2.16	1.414					
n	3	3	3	3	3	3	3	3	3	3	1	1	1	1	1
$t_{n-1,1-\frac{\alpha}{2}}$	4.3027	4.3027	4.3027	4.3027	4.3027	4.3027	4.3027	4.3027	4.3027	4.3027					
$t_{n-1,1-\frac{\alpha}{2}}\frac{S}{\sqrt{n-1}}$	2.48	2.48	2.87	3.79	3.79	6.57	7.99	9.40	6.57	4.30					
$\overline{V_y}-t_{n-1,1-\frac{\alpha}{2}}\frac{S}{\sqrt{n-1}}$	12.52	13.52	12.80	11.54	11.54	7.43	4.68	1.93	2.43	0					
$\overline{V_y}+t_{n-1,1-\frac{\alpha}{2}}\frac{S}{\sqrt{n-1}}$	17.48	18.48	18.54	19.12	19.12	20.57	20.66	20.73	15.57						

Table 12
Statistical values for calculation of the confidence interval for level $H = 40$ cm.

Distance from the symmetry axis [cm] / Statistical values	$x=0$	$x=1$	$x=2$	$x=3$	$x=4$	$x=5$	$x=6$	$x=7$	$x=8$	$x=9$	$x=10$	$x=11$	$x=12$	$x=13$	$x=14$	$x=15$	$x=16$
$\overline{V_y}$	11.33	12.33	13.33	14.5	14.33	14.50	12.83	11.67	10. 5	9.5	6.33	6.0	3.0	3.0	2.0	1.0	1.0
S	3.091	3.091	2.357	0.408	0.471	1.080	0.850	0.943	1.472	2.273	3.682	1.0	1.0				
n	3	3	3	3	3	3	3	3	3	3	3	2	2	1	1	1	1
$t_{n-1,1-\frac{\alpha}{2}}$	4.3027	4.3027	4.3027	4.3027	4.3027	4.3027	4.3027	4.3027	4.3027	4.3027	4.3027	12.706	12.706				
$t_{n-1,1-\frac{\alpha}{2}}\frac{S}{\sqrt{n-1}}$	9.40	9.40	7.17	1.24	1.43	3.29	2.59	2.87	4.48	6.92	11.20	12.71	12.71				
$\overline{V_y}-t_{n-1,1-\frac{\alpha}{2}}\frac{S}{\sqrt{n-1}}$	1.93	2.93	6.17	13.26	12.90	11.21	10.24	8.80	6.02	2.58	0	0	0				
$\overline{V_y}+t_{n-1,1-\frac{\alpha}{2}}\frac{S}{\sqrt{n-1}}$	20.73	21.73	20.50	15.74	15.76	17.79	15.42	14.37	14.98	16.42	17.57	18.71	15.71				

Table 13
Statistical values for calculation of the confidence interval for level $H = 50$ cm.

Distance from the symmetry axis x [cm]	Statistical values						
	$\overline{V_y}$	S	n	$t_{n-1,1-\frac{\alpha}{2}}$	$t_{n-1,1-\frac{\alpha}{2}}\frac{S}{\sqrt{n-1}}$	$\overline{V_y}-t_{n-1,1-\frac{\alpha}{2}}\frac{S}{\sqrt{n-1}}$	$\overline{V_y}+t_{n-1,1-\frac{\alpha}{2}}\frac{S}{\sqrt{n-1}}$
0	10.5	4.5	2	12.706	57.18	0	67.68
1	12.0	4.0	2	12.706	50.82	0	62.82
2	13.0	3.0	2	12.706	38.12	0	31.45
3	14.0	3.0	2	12.706	38.12	0	52.12
4	14.0	2.0	2	12.706	25.41	0	39.41
5	13.5	1.5	2	12.706	19.06	0	32.56
6	13.0	1.0	2	12.706	12.71	0.29	25.71
7	12.5	0.5	2	12.706	6.35	6.15	18.85
8	11.5	0.5	2	12.706	6.35	5.15	17.85
9	10.5	0.5	2	12.706	6.35	4.15	16.85
10	9.5	0.5	2	12.706	6.35	3.15	15.85
11	6.0	1.0	2	12.706	12.706	0	18.71
12	5.5		1				
13	4.0		1				
14	3.0		1				
15	2.5		1				
16	2.5		1				
17	2.0		1				
18	1.5		1				
19	1.5		1				
20	1.5		1				
21	1.0		1				

Notations

$\overline{V_y}$ average vertical velocity
S standard deviation [24,46]
α significance level
n number of readings
$t_{n-1,1-\frac{\alpha}{2}}$ quantile of Student's t distribution
$t_{n-1,1-\frac{\alpha}{2}}\frac{S}{\sqrt{n-1}}$ half of the confidence interval
$\overline{V_y}-t_{n-1,1-\frac{\alpha}{2}}\frac{S}{\sqrt{n-1}}$ lower limit of the confidence interval
$\overline{V_y}+t_{n-1,1-\frac{\alpha}{2}}\frac{S}{\sqrt{n-1}}$ upper limit of the confidence interval

Table 14
Statistical data for determination of the stagnant zone boundary.

Height H [cm]	Parameters of regression function and value x [cm]	Time t [s]				
		1	25	50	75	100
5	A_1 (A^*,a^{**})	18.71*	10.25	−12.28*	−16.22*	−10.67*
	B_1 (B^*,b^{**})	98.07*	10.25	86.43*	95.68*	73.01*
	C_1	–	−2.25	–	–	–
	r	0.998	–	0.988	0.965	0.985
	x	5.24	5.40	7.04	5.90	6.84
10	A_1 (A^*,a^{**})	−13.19*	−16.25	33.5**	11.8**	19.45
	B_1 (B^*,b^{**})	95.13*	20.25	−4.0**	−1.2**	−0.05
	C_1	–	−2.75	–	–	−0.25
	r	0.962	–	−0.97	−0.949	–
	x	7.21	6.45	8.38	9.84	8.72
20	A_1 (A^*,a^{**})	−11.07*	−22.8*	34.85**	−19.13*	
	B_1 (B^*,b^{**})	11.96*	−205.3*	−3.15**	203.5*	
	C_1	–	–	–	–	
	r	0.997	0.965	−0.919	0.978	
	x	10.80	9.0	11.06	10.6	
30	A_1 (A^*,a^{**})	−7.10*	−17.3*	−18.6*		
	B_1 (B^*,b^{**})	10.98*	198.4*	228.1*		
	C_1	–	–	–		
	r	0.963	0.875	0.933		
	x	15.50	11.50	12.3		
40	A_1 (A^*,a^{**})	−8.52*	−14.1*	−27.9*		
	B_1 (B^*,b^{**})	148.0*	184.8*	374.0*		
	C_1	–	–	–		
	r	0.96	0.837	0.954		
	x	17.4	13.1	13.4		

(continued on next page)

Table 14 (*continued*)

Height H [cm]	Parameters of regression function and value x [cm]	Time t [s]				
		1	25	50	75	100
50	A_1 (A^*,a^{**})	7.18**	30.4**			
	B_1 (B^*,b^{**})	−0.301**	−2.2**			
	C_1	–	–			
	r	−0.997	−0.914			
	x	23.8	13.82			
60	A_1 (A^*,a^{**})	−8.59	–			
	B_1 (B^*,b^{**})	1.33	–			
	C_1	−0.039	–			
	r	–	–			
	x	25.16	–			

References

[1] ENV, Part 4 2002 Eurocode 1, Actions on Silos and Tanks, 1991 Brussels, Belgium.
[2] ACI 313 1989.*Alternate Design Procedure,* Discussion Document before ACI Committee 313 on Concrete Bins, Silos and Bunkers for Storing Granular Materials, ACI, Detroit.
[3] AS 3774, Loads on Bulk Solids Containers, Australian Standards Association of Australia, Sydney, 1986.
[4] Polish Standard: *Silosy żelbetowe na materiały sypkie*, Obliczenia Statyczne, 1989, (in Polish).
[5] Anon 1985 *Reliable Flow of Particulate Solids*, EFCE Publication Series (European Federation of Chemical Engineers), 49.
[6] F. Ayuga, M. Guaita, P.J. Aguado, A. Couto, Discharge and the eccentricity of the hopper influence on the silo wall pressures, Journal of Engineering Mechanics 127 (10) (2001) 1067–1074.
[7] G.E. Blight, Eccentric discharge of a large coal bin with six outlets, Bulk Solids Handling 11 (2) (1991) 451–457.
[8] A. Borcz, el Rahim, Hamdy, Abd, Wall pressure measurements in eccentrically discharged cement silos, Bulk Solids Handling 11 (2) (1991) 469–476.
[9] J.W. Carson, Silo Failures: Case histories and Lessons Learned, Third Israeli Conference for Conveying and Handling of Particulate Solids, Dead Sea Israel, May 2000.
[10] J.F. Chen, J.M. Rotter, J.Y. Ooi, Z. Zhong, Flow patterns measurement in a full scale silo containing iron ore, Chemical Engineering Science 60 (2005) 3029–3041.
[11] J. Choi, A. Kudrolli, M.Z. Bazant, Velocity profile of granular flow inside silos and hoppers, Journal of Physics: Condensed Matter 17 (2005) S2533–S2548.
[12] C.S. Chou, J.Y. Hsu, Y.D. Lau, Flow patterns and stresses on the wall in a two-dimensional flat-bottomed bin, Journal of Chinese Institute of Engineers, Transactions of the Chinese Institute of Engineers, Series A 26 (4) (2003) 397–408.
[13] C.S. Chou, Y.C. Chuang, J. Smid, S.S. Hsiau, J.T. Kuo, Flow patterns and stresses on the wall in a moving granular bed with eccentric discharge, Advanced Powder Technology 13 (1) (2002) 1–13.
[14] C.S. Chou, J.Y. Hsu, Kinematic model for granular flow in a two-dimensional flat-bottomed hopper, Advanced Powder Technology 14 (3) (2003) 313–331.
[15] H. de Clercq, Investigation into Stability of a Silo with Concentric and Eccentric Discharge, Civil Engineers in South Africa 32 (3) (1990) 103–107.
[16] P.A. Cundall, O.D.L. Strack, A discrete numerical model for granular assemblies, Geotechnique 29 (1) (1979) 47–65.
[17] J.S. Guaita, A. Couto, F. Ayuga, Numerical simulation of wall pressure during discharge of granular material from cylindrical silos with eccentric hoppers, Biosystem Engineering 85 (1) (2003) 101–109.
[18] Hampe E, Kamiński M 1984 *Der Einfluss exzentrischer Entleerung auf die Druckverhealtnisse in Silos,* Bautechnik, Jg. 61, 1 H, 73–82, 2 H, 136–142
[19] U. Haussler, J. Eibl, Numerical investigations on discharging silos, Journal of Engineering Mechanics, Division ASCE 110 (EM6) (1984) 957–971.
[20] H.M. Haydl, Eccentric Discharge in Circular Silos, Proceedings of the Institution of Civil Engineers 83 (1987) 2.
[21] A.W. Jenike, Denting of circular bins with eccentric draw points, Journal of the Structural Division ASCE 93 (1967) 27–35 ST1.
[22] M. Kamiński, Der Betrieb von Silos mit exzentrischen Auslauf, Bautechnik Jg. 56 (H. 6) (1979) 203–204.
[23] M. Kamiński, Untersuchung des Zuckerdruckes in Silos: Tl 2. Exzentrische Entleerung, Zuckerindustrie Jg. 111 (10) (1986) 916–921.
[24] Z. Kotulski, W. Szczepiński, Rachunek błędów dla inżynierów, PWN, (Error Analysis with Applications in Engineering), 2004.
[25] M. Molenda, J. Horabik, S.A. Thompson, I.J. Ross, Bin loads induced by eccentric filling and discharge of grain, Transactions of the ASAE 45 (3) (2002) 781–785.
[26] R.M. Nedderman, U. Tüzün, A kinematic model for the flow of granular materials, Powder Technology 22 (1979) 243–253.
[27] K. Nübel, W. Huang, A study of localized deformation pattern in granular media, Computer Methods in Applied Mechanics and Engineering 193 (2004) 2719–2743.
[28] D.K. Pokrant, M.G. Britton, Investigation into the Effects of Eccentric Draw off and Flow rate in Model Grain Bin Studies, Paper-American Society of Agricultural Engineers (1986) 86–4076.
[29] J.M. Rotter, The Analysis of Steel Bins Subject to Eccentric Discharge, Proc., 2nd Inter. Conference on Bulk Materials Storage Handling and Transportation, Ins. of Eng, Wollongong, Australia, July 1986, pp. 264–271.
[30] J.M. Rotter, P.T. Jumikis, S.P. Fleming, S.J. Porter, Experiments on the Buckling of Thin-Walled Model Silo Structures, Research Report—University of Sydney, 1988, p. R570.
[31] J.M. Rotter, J.Y. Ooi, C. Lauder, I. Coker, J.F. Chen, B.G. Dale, A Study of the Flow Patterns in an Industrial Silo, Proceedings RELPOWFLO II, Oslo, August 1993, pp. 517–524.
[32] J.M. Rotter, Guide for the Economic Design of Metal Silos, E&FN Spon, London, 1998.
[33] K. Runesson, L. Nilsson, Finite element modelling of the gravitational flow of a granular material, Bulk Solids Handling 6 (5) (1986) 877–884.
[34] S.S. Safarian, E.C. Harris, Post-tensioned circular silos for modern industry, Bulk Solids Handling 7 (1987) 2.
[35] F. Shalouf, S. Kobielak, Reduction of the dynamic flow pressure in grain silo by using discharge tubes, Powder Handling Processing 13 (2001) 1.
[36] I. Sielamowicz, S. Błoński, T.A. Kowalewski, Optical technique DPIV in measurements of granular material flow, part 1 of 3 — plane hoppers, Chemical Engineering Science (2005) 589–598.
[37] I Sielamowicz, S Błoński, TA Kowalewski, Optical Technique DPIV in measurements of granular material flow, part 2 of 3 – converging hoppers, Chemical Engineering Science (2006).
[38] C. Slominski, M. Niedostatkiewicz, J. Tejchman, Application of particie image velocimetry (PIV) for deformation measurement during granular silo flow, Powder Technology 173 (2007) 1–18.
[39] C.Y. Song, J.G. Teng, Buckling of circular steel silos subject to code-specified eccentric discharge pressures, Engineering Structures 25 (2003) 1397–1417.
[40] J. Tejchman, Behaviour of granular medium in a silo — a numerical Cosserat approach, part 3, Archives of Civil Engineering 1 (1993) 7–28.
[41] J. Tejchman, Modelling of shear localisation and autogenous dynamic effects in granular bodies, Habilitation Monograph 140 (1997) 1–353 Veroffentlichungen des Institutes für Bodenmechanik und Felsmechanik der Universität Fridericiana in Karlsruhe.
[42] S.A. Thompson, J.L. Usry, J.A. Legg, Loads in a model grain bin as affected by various unloading techniques, Transactions of the ASAE 29 (1986) 2.
[43] U. Tüzün, R.M. Nedderman, Experimental evidence supporting kinematic modelling of the flow of granular media in the absence of air drag, Powder Technology 24 (2) (1979) 257–266.
[44] U. Tüzün, R.M. Nedderman, An investigation of the flow boundary during steady-state discharge from a funnel flow bunker, Powder Technology 31 (1) (1982) 27–43.
[45] G.R. Watson, J.M. Rotter, A finite element kinematic analysis of planar granular solids flow, Chemical Engineering Science 51 (16) (1996) 3967–3978.
[46] W. Volk, Applied Statistics for Engineers, second edition, by Mc Graw-Hill, 1969.
[47] M. Wójcik, G.G. Enstad, M. Jecmenica, Numerical calculations of wall pressures and stresses in steel cylindrical silos with concentric and eccentric hoppers, Journal of Particulate Science and Technology 21 (3) (2003) 247–258.
[48] J.G.M. Wood, The Analysis of Silo Structures Subject to Eccentric Discharge, Proc.,2nd Int. Conf. on Design of Silos for Strength and Flow, Stratford-upon-Avon, 1983, pp. 132–144.
[49] K.F. Zhang, J.Y. Ooi, A kinematic model for solids flow in flat bottomed silos, Geotechnique 48 (4) (1998) 545–553.
[50] G.M. Quenot, J. Pakleza, T.A. Kowalewski, Particle image velocimetry with optical flow, Experiments in Fluids 25 (1998) 177–189.